The Effect of Concentrated PV Gradients on Stationary Waves

RICHARD S. LINDZEN

Center for Meteorology and Physical Oceanography, Massachusetts Institute of Technology, Cambridge, Massachusetts

(Manuscript received 7 February 1994, in final form 14 April 1994)

ABSTRACT

The author reexamines the Charney–Drazin problem with special attention to the concentration of potential vorticity gradient in the neighborhood of the tropopause. It is found that the degree of concentration has a profound effect on the response to stationary forcing, with greater concentration leading to greater response. Smoothing the concentration either analytically or numerically (by using coarser resolution) both lead to reduced responses, especially at higher wavenumbers. The results suggest a potentially important interaction between baroclinically unstable eddies and stationary waves. Insofar as the former act to mix potential vorticity in the troposphere while concentrating gradients at tropopause levels, they significantly condition the basic state for the latter.

1. Introduction

While it has generally been understood that the restoring force for Rossby waves arises from meridional gradients of potential vorticity (PV), little attention has been given to the role of the detailed distribution of the potential vorticity gradient in determining the planetary-scale response to stationary forcing. Indeed, the classic work on this subject, Charney and Drazin (1961), focuses on the vertical propagation of such stationary waves in media where the PV gradient is order β, and this has been the general approach since then. However, it has recently been noted (Lindzen 1993; Sun and Lindzen 1994, and references therein) that PV gradients in the troposphere may be small even compared to β, while PV gradients are concentrated at large values at tropopause levels.

The purpose of the present paper is to examine the implications of such distributions of PV gradient for the atmospheric stationary wave response. It suffices for this purpose to use the simple model introduced by Charney and Drazin (1961). In section 2 we review this model and introduce a "standard" basic state wherein the troposphere is characterized by constant shear and static stability. We note that such a basic state is characterized by a tropospheric PV gradient on the order of 3β. We also introduce a basic state wherein the original basic state is adjusted to zero PV gradient in the troposphere. The resulting state involves almost unmeasurable alterations to the basic zonal flow U and temperature T. Nonetheless, the distribution of PV gradient is radically altered; not only is the tropospheric PV gradient eliminated, but the PV gradient at tropopause levels is greatly increased. In the present study we consider both these basic states as well as continuous variations between them. In section 3, we calculate the response to simple orographic surface forcing in this range of basic states. We find that the response, especially at higher zonal wavenumbers, depends profoundly on the degree of concentration of PV gradient at the tropopause, with higher concentrations generally leading to much larger responses. It should be added that none of the changes alter the propagation characteristics of stationary waves above the tropopause; however, overall amplitudes are pronouncedly affected.

The sensitivity to the concentration of PV gradient at the tropopause leads naturally to the question of what happens when either numerical or observational vertical resolution acts to smooth the concentration of PV gradient. We show, in section 4, that numerical smoothing of PV gradients leads to changes to response similar to what is obtained when high-resolution solutions are obtained for analytically smoothed basic states. In section 5, we examine the effect of concentrated PV gradient on the index of refraction for stationary waves. Not surprisingly, we find that concentrated PV gradients lead to ducts where even high zonal wavenumber waves can propagate and be reflected. This seems to be at the heart of the enhanced responses found when the concentrated PV gradients are taken into account. In section 6, we speculate on the interaction of unstable baroclinic transient waves, which act to

Corresponding author address: Dr. Richard S. Lindzen, Center for Meteorology and Physical Oceanography, Building 54, Rm. 1720, MIT, Cambridge, MA 02139.

mix PV with stationary waves by means of the conditioning of the basic state for the latter by the former. A simplified example of enhanced response in the presence of concentrated gradients is presented in an appendix.

2. Model description

Following Charney and Drazin (1961) we consider linearized waves on a zonally symmetric basic state in a quasigeostrophic fluid on a β-plane channel. The basic equation in such a system is the equation for the conservation of pseudo-potential vorticity; that is,

$$\left(\frac{\partial}{\partial t} + U\frac{\partial}{\partial x}\right)q' + v'\bar{q}_y = 0, \tag{1}$$

where

$$q' = \frac{1}{f_0}\left(\frac{\partial^2\Phi'}{\partial x^2} + \frac{\partial^2\Phi'}{\partial y^2}\right) + e^{z/H}\frac{\partial}{\partial z}\left(\frac{f_0}{N^2}e^{-z/H}\frac{\partial\Phi'}{\partial z}\right), \tag{2}$$

$$\frac{\partial\bar{q}}{\partial y} = -\frac{\partial^2 U}{\partial y^2} + \beta - e^{z/H}\frac{\partial}{\partial z}\left(\frac{f_0^2}{N^2}e^{-z/H}\frac{\partial U}{\partial z}\right). \tag{3}$$

Here U is the basic zonal flow, Φ' is the perturbation geopotential, and

$$u' = -\frac{1}{f_0}\frac{\partial\Phi'}{\partial y} \quad \text{and} \quad v' = \frac{1}{f_0}\frac{\partial\Phi'}{\partial x},$$

where u' and v' are the perturbation zonal and meridional velocities; f_0 is the Coriolis parameter, where $f = f_0 + \beta y$; and N^2, the square of the Brunt–Väisälä frequency, is given by

$$N^2 = \frac{g}{T}\left(\frac{dT}{dz} + \frac{g}{c_p}\right).$$

Here T is the basic temperature; H is a density scale height, taken to be constant; and x, y, z, and t are eastward, northward, and vertical distance, and time, respectively. For stationary waves, $\partial/\partial t \equiv 0$. Also, for present purposes, we will take U to be independent of y.

The energy equation relates Φ' to the vertical velocity w':

$$U\frac{\partial}{\partial x}\frac{\partial\Phi'}{\partial z} - \frac{\partial\Phi'}{\partial x}\frac{\partial U}{\partial z} + w'N^2 = 0. \tag{4}$$

Our stationary waves will be taken to be forced by orography of height h at the surface. Consistent with linearization, this implies

$$w' = U\frac{\partial h}{\partial x} \quad \text{at} \quad z = 0, \tag{5}$$

and together with (4), this leads to our lower boundary condition

$$U\frac{\partial}{\partial x}\frac{\partial\Phi'}{\partial z} - \frac{\partial\Phi'}{\partial x}\frac{\partial U}{\partial z} = -N^2U\frac{\partial h}{\partial x} \quad \text{at} \quad z = 0. \tag{6}$$

We will take h to be of the form

$$h = h(k)e^{ikx}\sin ly, \tag{7}$$

where we will assume $l = \pi/a$, a being the radius of the earth. For a β plane centered at latitude ϕ_0, k is related to the zonal wavenumber s by $k = s/a\cos(\phi_0)$. Since our present purpose is to examine the general response to stationary forcing, we will consider a continuous range of s, taking $h = 100$ m independent of s. For our upper boundary condition we will require either the radiation condition or boundedness as appropriate.

Given the form of (7), we can simplify (1) and (2) to obtain our vertical structure equation:

$$e^{z/H}\frac{d}{dz}\left(\frac{f_0^2}{N^2}e^{-z/H}\frac{d\Phi'}{dz}\right) + \left\{\frac{\bar{q}_y}{U} - (k^2 + l^2)\right\}\Phi' = 0, \tag{8}$$

where

$$\bar{q}_y = \beta - e^{z/H}\frac{d}{dz}\left(\frac{f_0^2}{N^2}e^{-z/H}\frac{dU}{dz}\right). \tag{9}$$

Our lower boundary equation becomes

$$U\frac{d\Phi'}{dz} - \frac{dU}{dz}\Phi' = -N^2Uh \quad \text{at} \quad z = 0. \tag{10}$$

The numerical solution of Eq. (8) is routine. Using centered differences, Eq. (8) is reduced to a second-order difference equation, which is solved by means of Gaussian elimination [see Lindzen (1990) for an explicit example]. We use an Arakawa–Moorthi grid (though the choice of grid proves largely irrelevant in this problem) wherein the first level is taken to be $1/2$ grid interval below $z = 0$. The lower boundary condition [Eq. (10)] is implemented between levels 1 and 2, while the finite-difference form of Eq. (8) is applied at level 2 and above. We found that numerical convergence was achieved for a vertical resolution of 100 m, and solutions with that resolution will be used as a basis for evaluating coarser resolutions. Although damping is not explicitly included in Eq. (8), we will consider the effect of simple linear damping of temperature and momentum associated with a timescale d^{-1}. This is trivially implemented by replacing U in Eq. (8) with

$$U - i\frac{d}{k}.$$

In most of the calculations we will present, we will use $d^{-1} = 100$ days, though the results do not significantly vary from those obtained with $a = 0$.

TABLE 1. Parameters for vertical structure.

j	z_j (km)	ϵ_j (km)	$\left.\frac{dT}{dz}\right\|_j$ (K/km)	$\left.\frac{dU}{dz}\right\|_j$ (m s^{-1}/km)
0	10			
1	12	2	0	−1.5
2	24	4	2.8	0.7
3	50	2	0	0

Essential to the present paper is our choice of basic state. We turn to this matter next.

Unadjusted and adjusted basic states

We begin with a simple approximation to a standard atmosphere below 50 km. Above 50 km, we take U and T constant at their values for 50 km. This is, of course, unrealistic, but in this paper we are not concerned with the upper mesospheric response, and the choice facilitates the imposition of the radiation condition. This state will be referred to as our unadjusted basic state. Below 10 km, this state is characterized by a constant shear and a constant N^2. Taking N^2 constant implies that the easily calculated dT/dz differs slightly from a constant. We choose $U(0) = 5$ m s^{-1}, $T(0) = 285$ K, $dU/dz = 2.2$ m s^{-1}/km, and $T(10 \text{ km}) = 220$ K. Above 10 km we use the following expressions for dU/dz and dT/dz:

$$\frac{dU}{dz} = \left.\frac{dU}{dz}\right|_0 + \sum_{j=1}^{3} \left(\frac{1 + \tanh\left(\frac{z - z_j}{\epsilon_j}\right)}{2} \right) \times \left(\left.\frac{dU}{dz}\right|_{j-1} - \left.\frac{dU}{dz}\right|_j \right), \quad (11)$$

and

$$\frac{dT}{dz} = \left.\frac{dT}{dz}\right|_0 + \sum_{j=1}^{3} \left(\frac{1 + \tanh\left(\frac{z - z_j}{\epsilon_j}\right)}{2} \right) \times \left(\left.\frac{dT}{dz}\right|_{j-1} - \left.\frac{dT}{dz}\right|_j \right). \quad (12)$$

The values $d/dz|_j$ refer to nominal values of the derivative, which are chosen for levels z_j. It is, however, clear from Eqs. (11) and (12) that these are not the values at $z = z_j$, but are smoothly approached for $z > z_j$ with a scale ϵ_j. Level z_0 is 10 km, and values for derivatives at this level are taken from the assumed profiles below 10 km. Our parameter choices are given in Table 1. Here U and T are obtained by integrating Eqs. (11) and (12), assuming continuity at 10 km. This procedure allows slight discontinuities in derivatives at $z = 10$ km which, in turn, leads to thin spikes in $\bar{q}_y$. In order to avoid these spikes, we replaced the above-de-

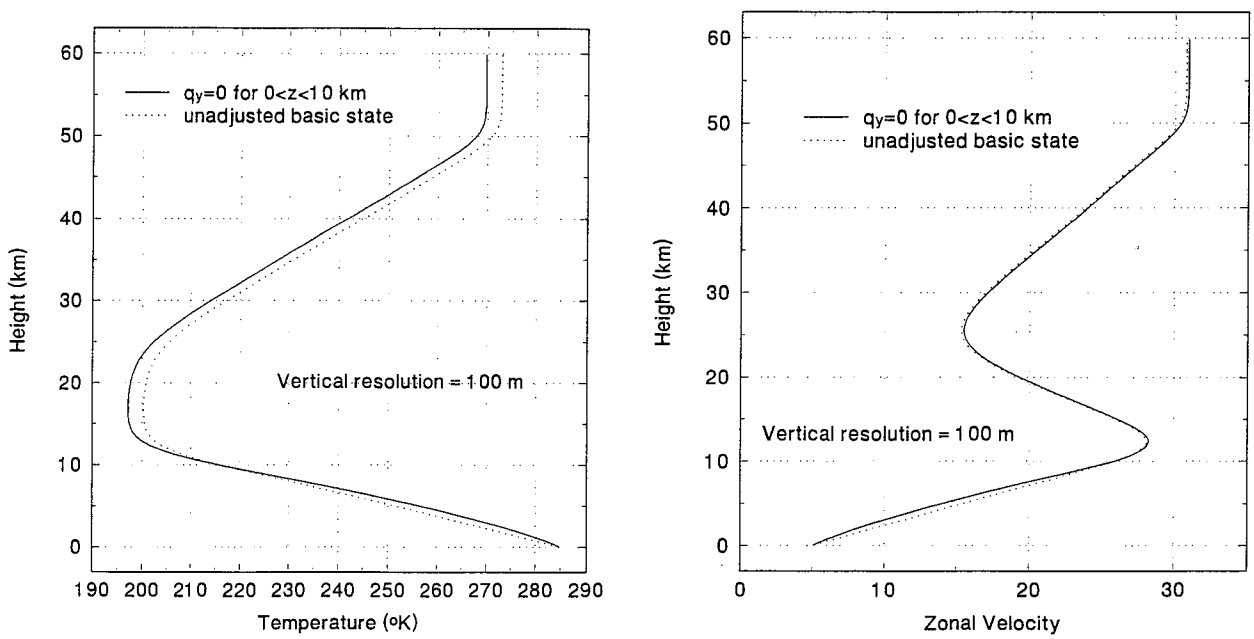

FIG. 1. Basic temperature (a) and zonal velocity (b) as a function of z. Dotted line shows unadjusted profile, while solid line shows profile adjusted to produce $\bar{q}_y = 0$ below 10 km.

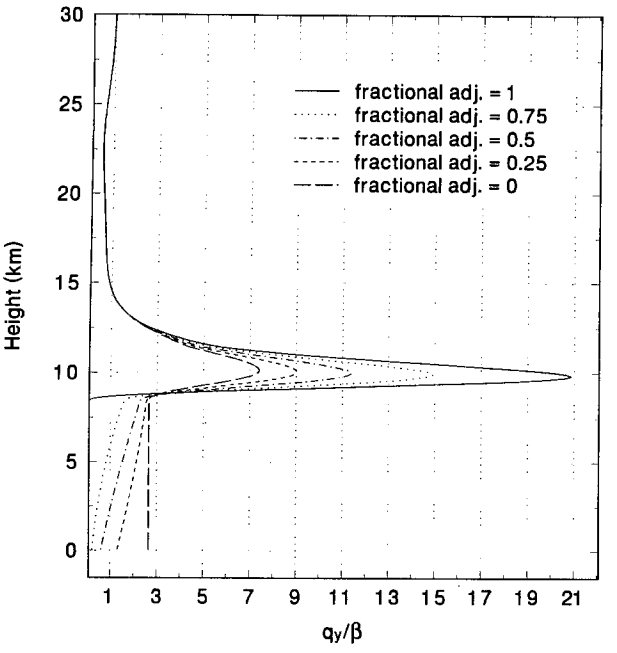

FIG. 2. Plot of $\bar{q}_y$ scaled by β calculated from basic U and T fields with varying degrees of adjustment.

scribed curves between $z = 8.5$ and 11.5 km with sixth-order polynomial fits, which preserved continuity of the functions and their first two derivatives. While this eliminated the spikes in $\bar{q}_y$, it had no visible effect on the calculated stationary wave response. The resulting basic state is shown in Fig. 1. We next consider an alteration of this state wherein U and T are modified so as to bring $\bar{q}_y$ to zero below 10 km. From Eq. (3), this requires

$$\frac{d}{dz}\left(\frac{f_0^2}{N^2}e^{-z/H}\frac{dU}{dz}\right) = \beta e^{-z/H}, \tag{13}$$

which may be integrated to yield

$$\frac{f_0^2}{N^2}\frac{dU}{dz} = \beta H(e^{z/H} - 1) + e^{z/H}\frac{f_0^2}{N^2(0)}\frac{dU}{dz}\bigg|_{z=0}. \tag{14}$$

Clearly, there is no unique solution to Eq. (14). For example, one could modify N^2 while keeping dU/dz constant, or vice versa, or some combination of the two. As it turns out, it does not make much difference in the present problem. Solving for N^2 while keeping dU/dz constant yields

$$N^2 = N^2(0)\left\{\left[\beta H\Big/\left(\frac{f_0^2}{N^2(0)}\frac{dU}{dz}\right) + 1\right] \times (e^{z/H} - 1) + 1\right\}^{-1}. \tag{15}$$

We can, instead, partially adjust N^2, replacing Eq. (15) with

$$N^2 = N^2(0)\left\{\alpha\left[\beta H\Big/\left(\frac{f_0^2}{N^2(0)}\frac{dU}{dz}\right) + 1\right] \times (e^{z/H} - 1) + 1\right\}^{-1}, \tag{16}$$

where $\alpha < 1$. Then dU/dz must be modified to

$$\frac{dU}{dz} = \frac{dU}{dz}\bigg|_{z=0}\frac{\lambda(e^{z/H} - 1) + e^{z/H}}{1 + \alpha(\lambda + 1)(e^{z/H} - 1)}, \tag{17}$$

where

$$\lambda = \beta H\Big/\left(\frac{f_0^2}{N^2(0)}\frac{dU}{dz}\bigg|_{z=0}\right).$$

We can choose $N^2(0)$ and $dU/dz|_0$ so that $U(0)$, $T(0)$, U (10 km), and T (10 km) remain the same as in the unadjusted state. In addition, we again replace the fields between $z = 8.5$ and 11.5 km with sixth-order polynomial fits, which preserve continuity of the func-

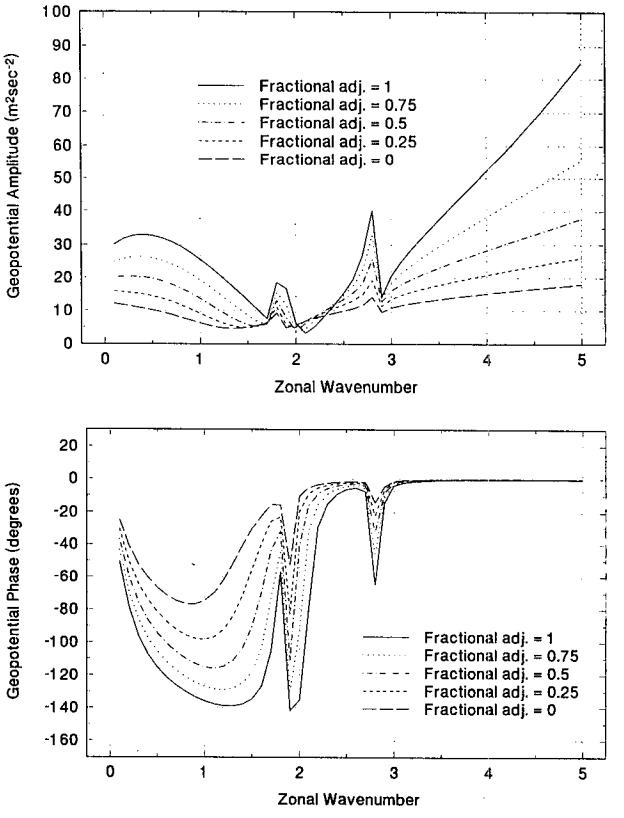

FIG. 3. Amplitude (a) and phase (b) of geopotential response at the surface to stationary forcing as a function of zonal wavenumber s for various degrees of adjustment.

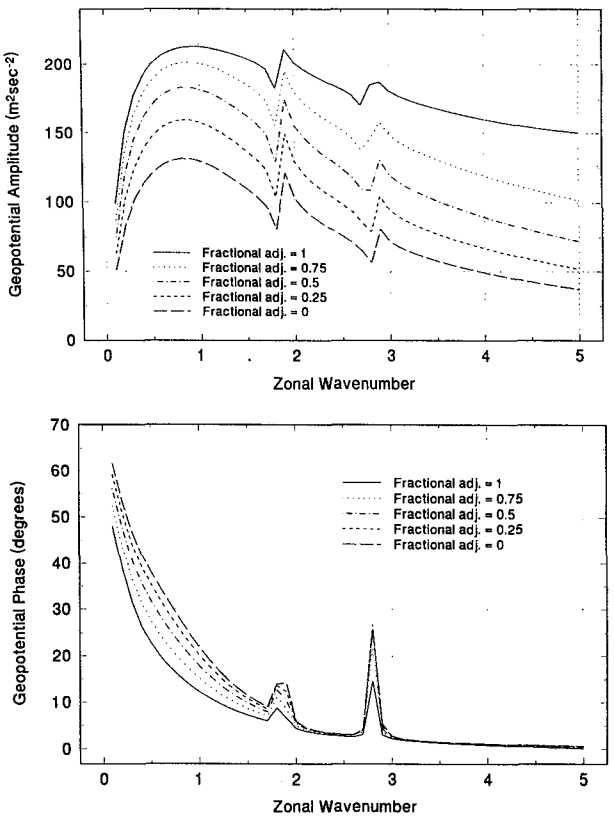

FIG. 4. Same as Fig. 3 but for response at 10 km.

tions and their first two derivatives. The particular choice of α (between 0 and 1) had no significant effect on our results, which is not surprising given that $\bar{q}_y$ is the main determinant of wave behavior. The results for $\alpha = 0.45$ are shown in Fig. 1. Interestingly, the adjusted state seems to differ almost negligibly from the unadjusted state. However, this is *not* because the unadjusted state already has a small $\bar{q}_y$; it does not. The vertical distribution of $\bar{q}_y$ (evaluated numerically with a 100-m resolution) is shown in Fig. 2 for both adjusted and unadjusted states. For the unadjusted state, $\bar{q}_y \approx 2.7 \times \beta$. On the other hand, the magnitude of the peak $\bar{q}_y$ above 10 km is much greater for the adjusted state.

Finally, we will consider basic states that represent a continuous transition between the unadjusted and fully adjusted states. These are given by

$$\begin{pmatrix} U \\ T \end{pmatrix} = \mu \begin{pmatrix} U_{\text{adjusted}} \\ T_{\text{adjusted}} \end{pmatrix} + (1 - \mu) \begin{pmatrix} U_{\text{unadjusted}} \\ T_{\text{unadjusted}} \end{pmatrix}, \quad (18)$$

where $1 \geq \mu \geq 0$. In Fig. 2 we show the changes in the distribution of $\bar{q}_y$ associated with $\mu \neq 1$. We see that even $\mu = 0.75$ is associated with substantial values of $\bar{q}_y$ in the troposphere. The simple results we have just seen suggest the difficulty in determining $\bar{q}_y$ from data. This is particularly true for data from a single latitude. However, as noted by Sun and Lindzen (1994), $\bar{q}_y$ is essentially the slope of isentropic surfaces, and even small slopes lead to substantial changes in the elevation of an isentrope as one moves from the Tropics to the pole. Thus, it is possible to pin down values of $\bar{q}_y$ to a greater extent than the present calculations suggest. Sun and Lindzen's analysis suggests that $\bar{q}_y \leqslant O(\beta)$ through the bulk of the extratropical troposphere.

3. Response to stationary forcing for varying degrees of adjustment

As is frequently the case, the volume of results that would be required to clearly display all the effects of smoothing PV gradients in the troposphere while concentrating them in the neighborhood of the tropopause exceeds what is practical to present in a paper. In the present case, this is not so serious since the calculations are sufficiently simple that most interested readers could readily replicate them. We will attempt to select results that seem sufficient to characterize the general picture. Figures 3–5 show the amplitude and phase of Φ' as a function of zonal wavenumber for various choices of μ at the surface, 10 km, and 25 km, respec-

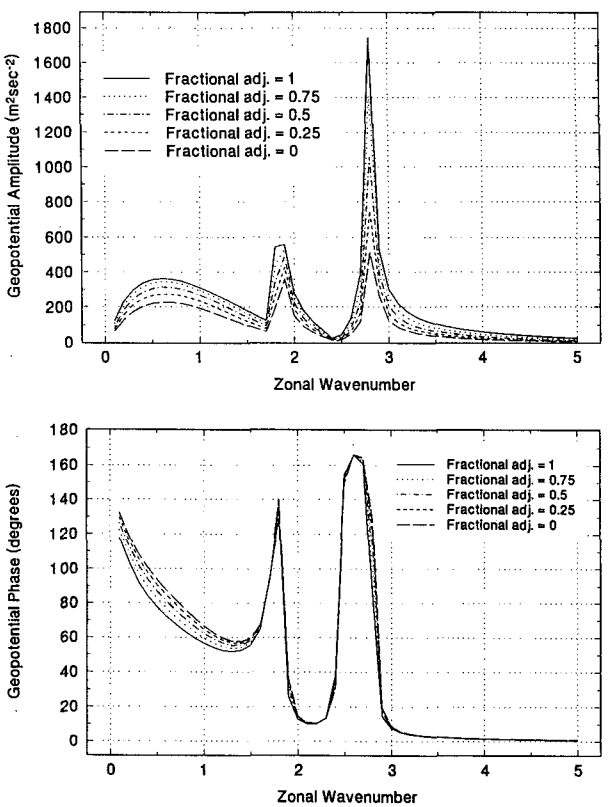

FIG. 5. Same as Fig. 3 but for response at 25 km.

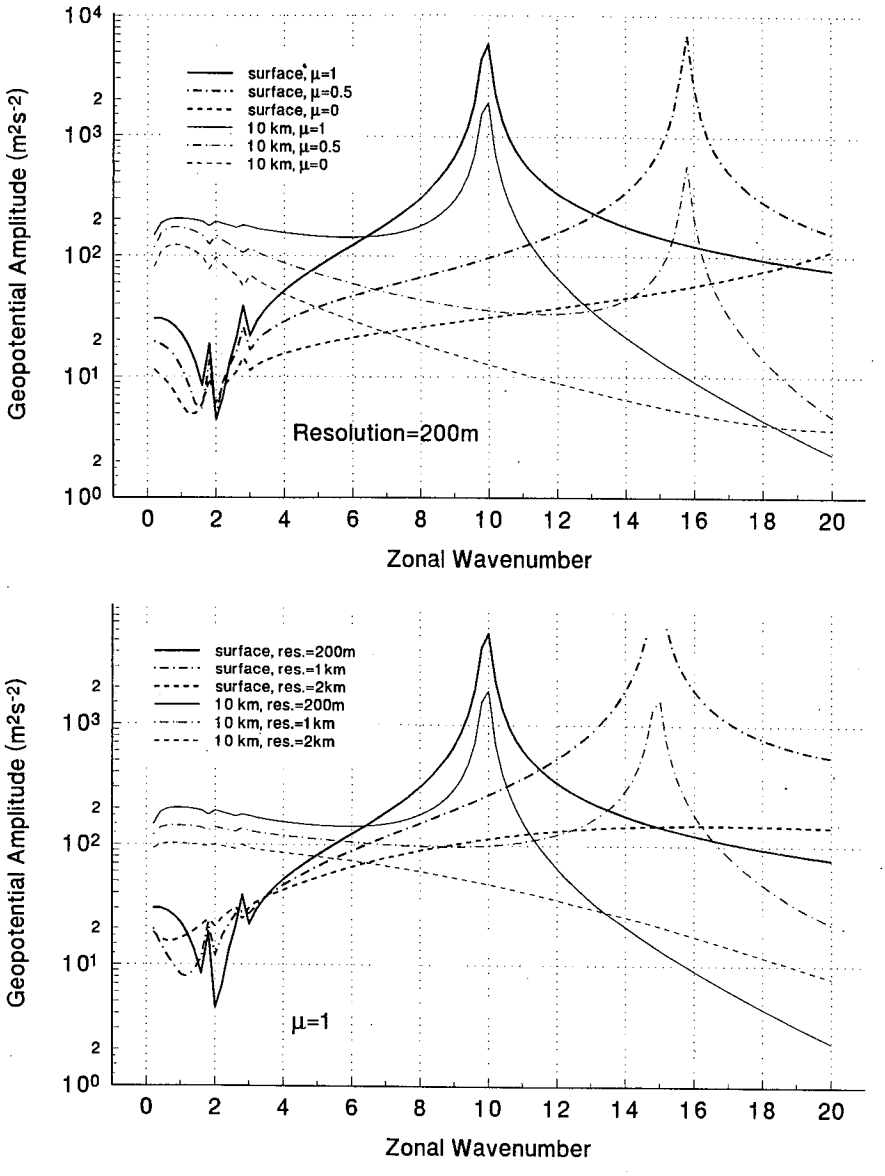

FIG. 6. Amplitude of the geopotential response (a) as function of zonal wavenumber and (b) as a function of resolution at the surface and at 10 km as a function of μ. This figure uses a logarithmic scale and extends to higher wavenumbers.

tively. At all levels we see that amplitudes tend to increase very substantially as μ approaches 1, the effect being most pronounced at higher wavenumbers, though by 25 km the responses at these wavenumbers are small because of increased trapping. The behavior at 25 km is characteristic of all levels above the tropopause. Phase changes are modest except at the surface. There is clear evidence of resonant-like behavior below wavenumbers 2 and 3 regardless of μ; this behavior is similar to what was found by Lindzen (1994) for the Eady Problem modified by the presence of β. The nature of these resonances is discussed in the appendix, where we consider a highly simplified problem that displays many of the features of the present problem but is easily solved analytically. These resonances appear to arise from the partial reflection in the region of concentrated $\bar{q}_y$ of waves that can propagate or tunnel in the troposphere.[1] Propagation properties are described in section

[1] Even when the region below the tropopause does not sustain propagation at a given wavenumber, there is always a region in the neighborhood of the lower boundary that does (if only because the lower boundary condition implies a δ function in $\bar{q}_y$ at the surface

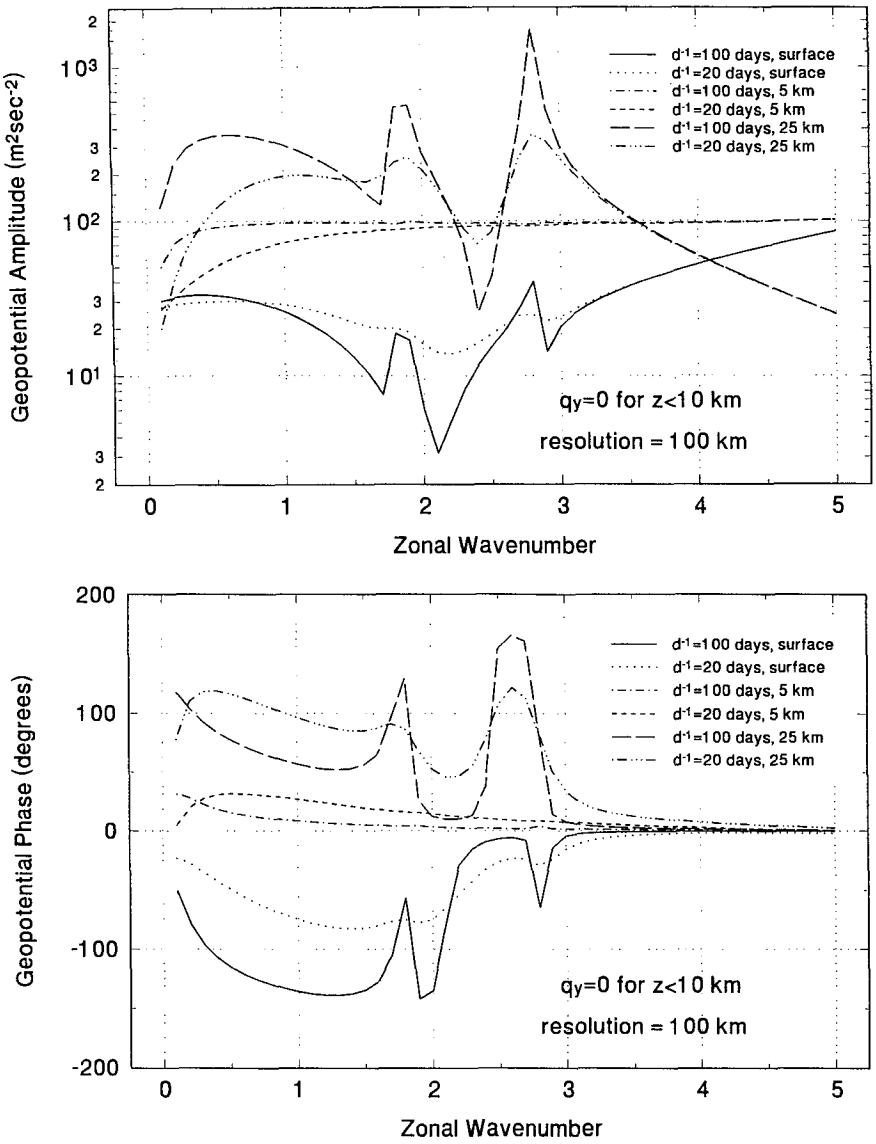

FIG. 7. Amplitude (a) and phase (b) of geopotential response to stationary forcing for fully adjusted basic state at 0, 5, and 25 km for damping times of 100 and 20 days.

5. The growing response with increasing s is due to an additional resonant response at wavenumbers higher than we have displayed. The situation is illustrated in Fig. 6a. We see that this resonance moves to higher wavenumbers as μ approaches zero. An analysis of this phenomenon is also given in the appendix. This high wavenumber resonance appears to be associated with waves that are ducted in the region of concentrated $\bar{q}_y$. It should be noted that we are using forcing independent of s in the present calculation. In reality, the forcing diminishes markedly with increasing s so that the increasing response found here need not be troubling. The present results, however, do suggest that failure to resolve the concentration of PV gradient in the neighborhood of the tropopause could lead to underestimating the finer structure of stationary waves near the surface. The effects of reduced resolution will be treated in greater detail in the following section.

Returning to the phase changes for a moment, the phase changes indicated in Fig. 3 for the surface are,

where all wavenumbers can "propagate"). Thus, the upper-level concentration in $\bar{q}_y$ can provide both a duct for waves trapped in the body of the troposphere and a partial reflector for waves tunneling between the ducts at the surface and in the neighborhood of the tropopause.

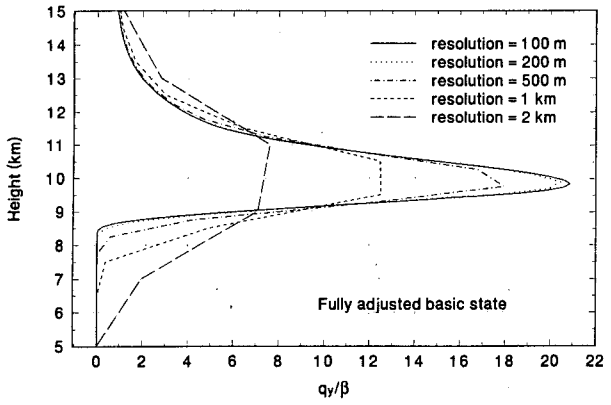

FIG. 8. Plot of $\bar{q}_y$ scaled by β calculated from fully adjusted basic state using various resolutions.

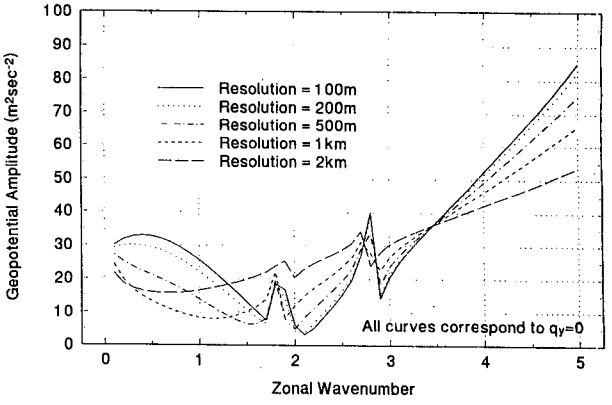

FIG. 10. Amplitude of geopotential response at the surface to stationary forcing as a function of zonal wavenumber s for fully adjusted basic state and various resolutions.

in fact, major for wavenumbers 1 and 2. Even at 25 km, where the phase changes associated with varying μ are small, the major phase changes associated with the "resonant" peaks are potentially important even though they appear to occur away from the realizable integer values of s. The fact of the matter is that the wavenumbers vary with the assumed channel width, the mean flow, etc. Thus, the existence of such peaks near realizable wavenumbers suggests the possibility of major shifts in response as the basic-state changes.

The existence of resonant behavior is always sensitive to the existence of dissipation. We have found that the presence of dissipation does alter this behavior. This can be seen in Fig. 7, where responses for $d^{-1} = 100$ days are compared with responses for $d^{-1} = 20$ days. As might be expected, damping only affects wavenumbers for which propagation exists away from the tropopause region. Higher wavenumbers are negligibly affected, though even these modes can propagate in the neighborhood of the tropopause. This will be discussed in greater detail in section 5. Interestingly, however, even for $a^{-1} = 20$ days, the response sensitivity to varying μ remains large.

4. Effect of resolution on calculated responses

We have seen in the preceding section how the concentration of PV gradient near the tropopause can profoundly affect the atmospheric response at all levels to stationary forcing at the surface. While we have used analytic specifications for U and T; $\bar{q}_y$ was evaluated using finite differences over a 100-m grid interval. Obviously, using a coarser grid interval will act to smooth out the peak in the PV gradient. Relatedly, the observed gradient is constrained by the coarseness of the observational sampling. In Fig. 8 we show how increasing vertical grid interval acts to smooth $\bar{q}_y$ when $\mu = 1$. Comparison with Fig. 2 shows that the effect is similar to reducing μ. Of course, even for $\mu = 0$ there is a peak

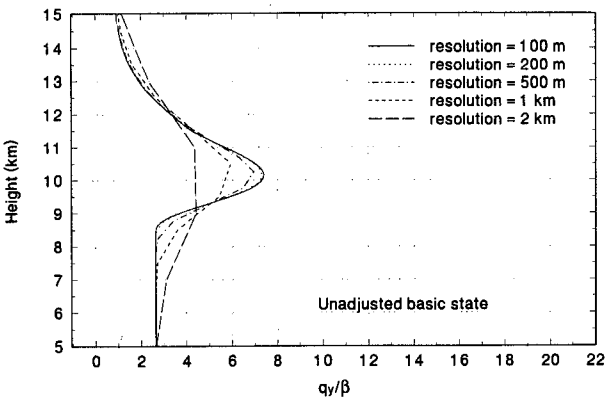

FIG. 9. Same as Fig. 8 but for unadjusted basic state.

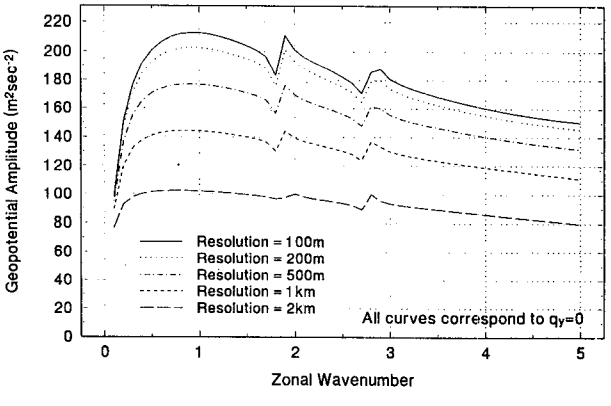

FIG. 11. Same as Fig. 10 but for response at 10 km.

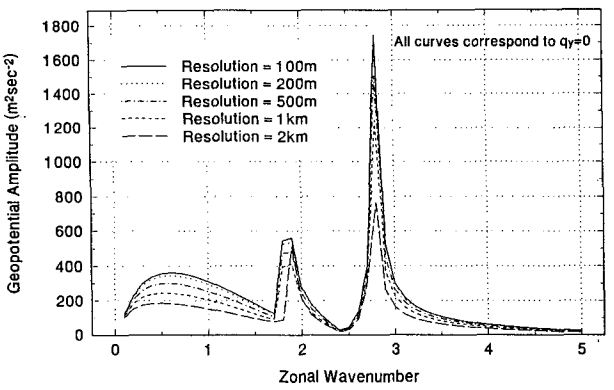

FIG. 12. Same as Fig. 10 but for response at 25 km.

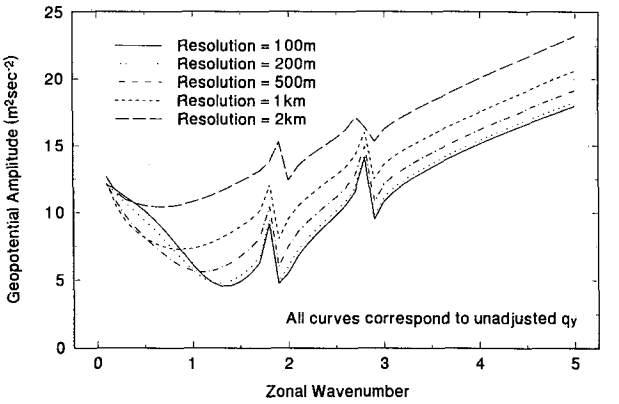

FIG. 13. Same as Fig. 10 but fof unadjusted basic state.

in $\bar{q}_y$ near 10 km and, as shown in Fig. 9, this peak too will be reduced by coarse resolution.

In general, the effect of coarse resolution in the numerical solution of Eq. (8) is similar to what we obtained by reducing μ—except at the surface. This is seen in Figs. 10, 11, and 12 for the surface, 10 km, and 25 km, respectively. At the surface, the response at some wavenumbers actually increases with coarser resolution. Similar results were found in the preceding section where dissipation sometimes increased the surface response. Such behavior is indicative of destructive interference due to upper-level reflections. Presumably both coarser resolution and dissipation act to reduce reflections, which lead to destructive interference. Reference to Fig. 6b shows that the high wavenumber resonance mentioned in section 3 is affected by decreasing resolution in almost the same manner as it was by decreasing μ. However, the coarsest resolution (2 km) seems to kill this resonance, whereas $\mu = 0$ seems to only move it to still higher wavenumbers.

A somewhat surprising result is found when one considers resolution broadening for the case where $\mu = 0$. Results at the surface for this case are shown in Fig. 13. Here, response generally increases as resolution becomes coarser. This effect is found only within a few kilometers of the surface. As we see in Fig. 14 for 10 km, response again decreases with poorer resolution.

It should be emphasized that all the resolutions we use—even 2 km—are considered to be reasonably high resolutions by GCM standards. Indeed, all these resolutions are entirely adequate to resolve the gross propagation characteristics of stationary waves. This is clearly illustrated in Fig. 15, where we show the vertical structure of the $s = 1$ response for various resolutions. It is evident that the phase distribution is well represented by all resolutions. Similarly, the *structure* of the amplitude is well represented by all resolutions. Only the concentration of PV gradient near the tropopause is poorly resolved (as are, presumably, the waves within the duct formed in this region); however, this has a profound effect on overall amplitude. It is interesting in this regard that GCM modelers at NASA's Goddard Space Flight Center have found that increasing model vertical resolution in the neighborhood of the tropopause led to immense improvement in stationary wave simulations (S. Schubert and A. Y. Hou 1993, personal communication).

5. Index of refraction as affected by adjustment and resolution

It is commonly noted (Charney and Drazin 1961; Holton 1975; Lindzen 1990; and many others) that for winter westerlies, stationary waves can propagate for wavenumbers 1, 2, and sometimes 3, but for higher wavenumbers the waves are trapped. This is generally so. However, the concentration of $\bar{q}_y$ near the tropopause produces a shallow duct where much higher wavenumbers can locally propagate. The bracketed quantity in Eq. (8) is essentially an index of refraction.

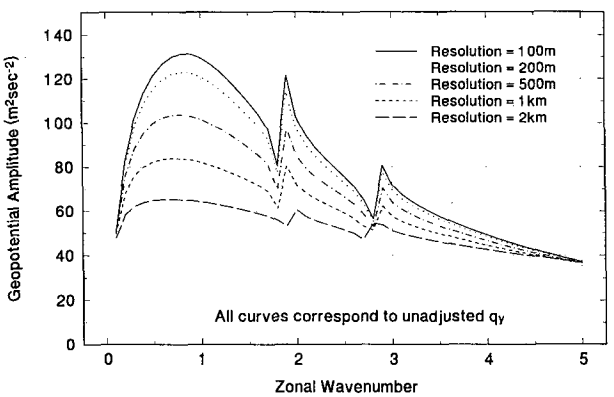

FIG. 14. Same as Fig. 11 but for unadjusted basic state.

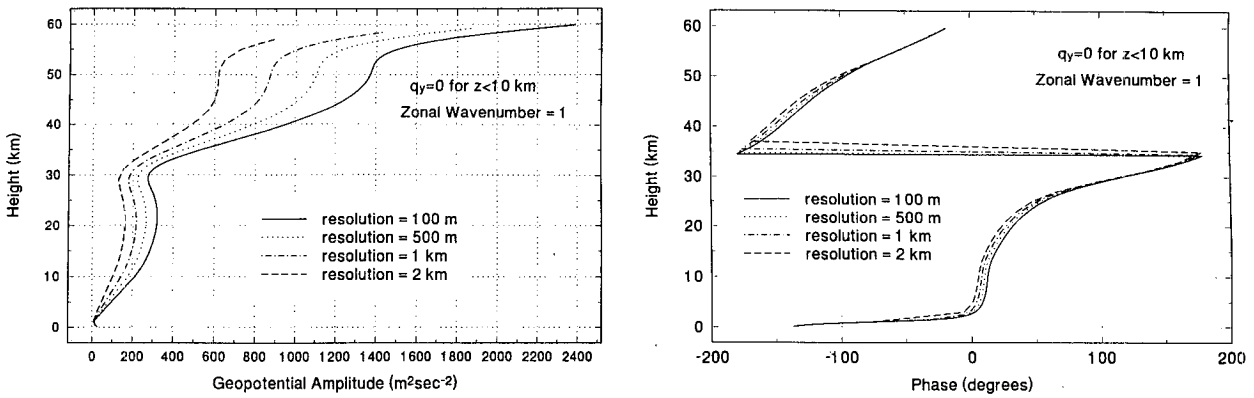

FIG. 15. Amplitude (a) and phase (b) of geopotential response to stationary forcing as a function of z for $s = 1$, a fully adjusted basic state, and various resolutions.

Clearly, as s (or equivalently k) increases, the index of refraction will eventually turn negative. We may refer to the value of s at which this occurs as s_{cutoff}; s_{cutoff} is a function of z. In Fig. 16 we show how s_{cutoff} varies as μ decreases from 1 to zero while evaluating $\bar{q}_y$ and N^2 with a resolution of 100 m. In Fig. 17 we show how changing resolution affects s_{cutoff} when $\mu = 1$. In both cases the nature of the duct is significantly altered. However, the changes are somewhat different for the two cases. Among these differences is the fact that for small values of μ there is some potential for ducting near the surface due to the small value of U.

6. Remarks

The purpose of this paper is not the precise calculation of stationary waves, but rather to note that the existence of a shallow region of concentrated PV gradient in the neighborhood of the tropopause can have profound influence on the overall magnitude of stationary waves without necessarily affecting the overall structure of the wave. The degree of concentration present in our idealized basic states may, in fact, be greater than actually occurs, but we cannot tell unless the data have sufficient resolution. In solving the equations numerically, the numerical resolution also limits the degree of concentration that can be "seen" with effects similar to what is obtained when the concentration of PV gradient is analytically smoothed.

In practice, baroclinically unstable eddies act to mix PV within the troposphere (Held and Hoskins 1985; Marshall and Nurser 1991), leading to concentrations of gradients at the surface and at the upper limit of mixing. According to Lindzen (1993), mixing to a sufficiently great level (approximately the tropopause) can neutralize the fluid with respect to baroclinic instability. The interesting possibility arises that the more intense the unstable transient eddies, the greater the degree of concentration of PV gradients in the neighborhood of the tropopause and the greater the stationary

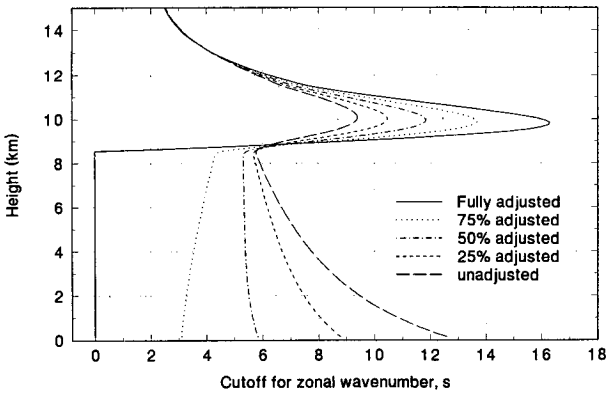

FIG. 16. Plot of s_{cutoff} as a function of z for various degrees of adjustment. See text for details.

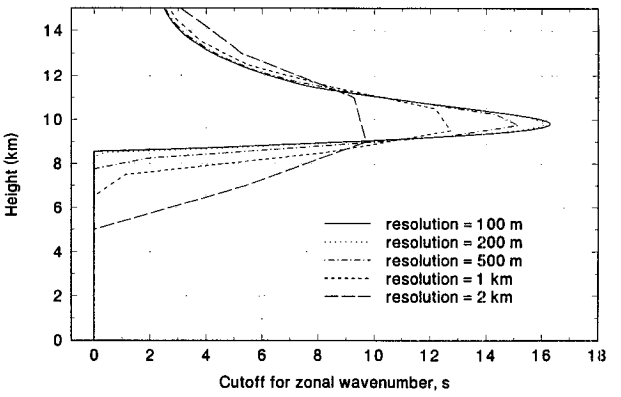

FIG. 17. Same as Fig. 16 but for fully adjusted basic state and varying resolution.

wave response. This suggests that a major interaction of unstable transient eddies and stationary waves results from the former conditioning the basic state for the latter, quite apart from the direct interaction of the two types of eddies. It has been noted (Hou and Lindzen 1992) that the more intense the Hadley circulation, the greater the PV gradients at the winter edge of the Hadley circulation, and these increased gradients could lead to stronger eddy activity. Some numerical support for this suggestion was found by Hou (1993) and Hou and Molod (1994). The strength of the Hadley circulation appears to depend on the distance of the zonally averaged surface temperature maximum from the equator (Lindzen and Hou 1988) and on the degree of meridional concentration of zonally averaged heating (Hou and Lindzen 1992). Orbital variations and tectonic changes affect these quantities greatly over paleoclimatic timescales (Lindzen and Pan 1994). However, on shorter timescales, El Niño–Southern Oscillation events can also play a role. Here, it is important to note that the present results suggest that the effect of El Niño–Southern Oscillation events may be to enhance the response of the atmosphere to stationary forcing (especially at higher wavenumbers) rather than to contribute specifically to the forcing of stationary waves. To the best of our knowledge, no current data analyses have been designed to examine this possibility.

Acknowledgments. This work was supported by Grant 914441-ATM from the National Science Foundation and Grant NAGW 525 from the National Aeronautics and Space Administration. Fifteen percent of this research was funded by the U.S. Department of Energy's (DOE) National Institute of Global Environmental Change (NIGEC) through the NIGEC Northeast Regional Center at Harvard University (DOE Cooperative Agreement DE-FC03-90ER61010). Financial support does not constitute an endorsement by DOE of the views expressed in this article. Helpful suggestions from Dr. Edmund K. M. Chang are gratefully acknowledged.

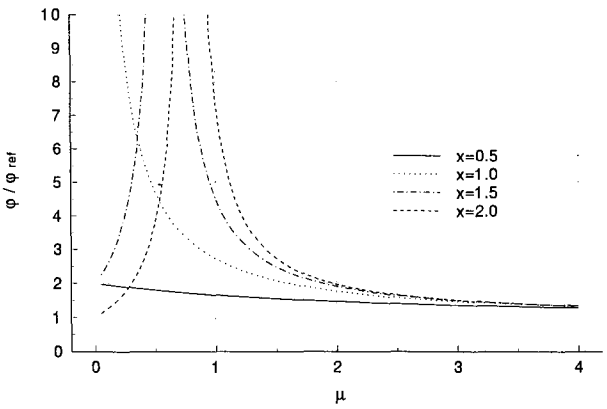

FIG. A1. Magnitude of relative response as a function of μ for various choices of $\bar{x}$. See appendix for details.

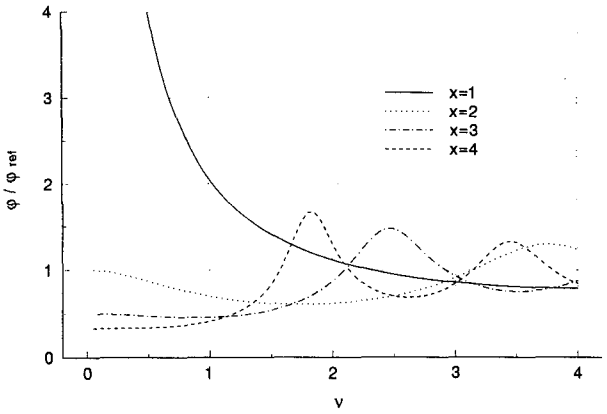

FIG. A2. Magnitude of relative response as a function of ν for various choices of $\bar{x}$. See appendix for details.

APPENDIX

Simple Analytic Model

Many of the effects we have noted in the Charney–Drazin model can be seen in a simple analytic model wherein we have a constant index of refraction background plus a delta function contribution at some level. The equation we consider is

$$\frac{d^2\phi}{dz^2} + (\lambda_1\delta(z - z_0) - \lambda_2^2)\phi = 0, \qquad (19)$$

with a simple lower boundary condition

$$\phi(0) = 1.$$

We will initially assume that waves are trapped away from the δ-function contribution, that is, $\lambda_2^2 > 0$. The solution to Eq. (19) when $\lambda_1 = 0$ is

$$\phi = e^{-\lambda_2 z}. \qquad (20)$$

We will use (20) as our reference solution in order to see whether the presence of the δ-function contribution increases or diminishes the response. When $\lambda_1 \neq 0$, our solution to (19) is

$$\phi = A_1 e^{-\lambda_2(z-z_0)} \quad \text{for} \quad z > z_0,$$

and

$$\phi = \cosh(\lambda_2 z) + A_0 \sinh(\lambda_2 z) \quad \text{for} \quad z < z_0. \qquad (21)$$

Assuming continuity for ϕ at $z = z_0$, integrating (19) across z_0 gives us the discontinuity in $d\phi/dz$ at $z = z_0$:

$$\left.\frac{d\phi}{dz}\right|_{z_0-}^{z_0+} + \lambda_1\phi(z_0) = 0. \qquad (22)$$

Continuity together with (22) allow us to solve for A_0 and A_1. For the purposes of this appendix, it suffices to simply solve for the ratio of our solution to the reference solution given by (20) for the region above z_0:

$$\frac{\phi}{\phi_{\text{ref}}} = \left[1 - \frac{\lambda_1}{2\lambda_2}(1 - e^{-2\lambda_2 z_0})\right]^{-1}. \qquad (23)$$

For convenience of presentation, we introduce the following definitions: $\mu \equiv 2\lambda_2/\lambda_1$, and $\bar{x} \equiv \lambda_1 z_0$. (Here μ obviously has nothing to do with μ used in the body of the text. There it served as an adjustment parameter for the basic state.) Equation (23) becomes

$$\frac{\phi}{\phi_{\text{ref}}} = \left[1 - \frac{1}{\mu}(1 - e^{-\mu\bar{x}})\right]^{-1}.$$

We display the magnitude of ϕ/ϕ_{ref} as a function of μ for various choices of $\bar{x}$ in Fig. A1. Note the presence of resonances and that the relative response is, in the figure, always greater than one (though, of course, for small enough μ and large enough $\bar{x}$ the ratio can even turn negative). The situation is analogous to the high wavenumber resonance shown in Fig. 6. Here the δ function is providing a resonating duct. To consider the case when the background index of refraction is positive, we simply let $\mu = i\nu$. The magnitude of the relative response as a function ν for various choices of $\bar{x}$ is shown in Fig. A2. Here we see less dramatic resonant responses where the region below z_0 is the duct with the δ-function region providing partial reflection. These responses are analogous to the resonance-like responses found earlier at small values of s.

REFERENCES

Charney, J. G., and P. G. Drazin, 1961: Propagation of planetary-scale disturbances from the lower into the upper atmosphere. *J. Geophys. Res.*, **66,** 83–110.

Held, I. M., and B. J. Hoskins, 1985: Large-scale eddies and the general circulation of the troposphere. *Advances in Geophysics,* Vol. 28A, Academic Press, 3–31.

Holton, J. R., 1975: *The Dynamic Meteorology of the Stratosphere and Mesosphere. Meteor. Monogr.,* No. 37, Amer. Meteor. Soc., 216 pp.

Hou, A. Y., 1993: The influence of tropical heating displacements on the extratropical climate. *J. Atmos. Sci.,* **50,** 3553–3570.

——, and R. S. Lindzen, 1992: The influence of concentrated heating on the Hadley circulation. *J. Atmos. Sci.,* **49,** 1233–1241.

——, and A. Molod, 1994: Modulation of dynamic heating in the winter extratropics associated with the cross-equatorial Hadley circulation. *J. Atmos. Sci.,* submitted.

Lindzen, R. S., 1990: *Dynamics in Atmospheric Physics.* Cambridge University Press, 310 pp.

——, 1993: Baroclinic neutrality and the tropopause. *J. Atmos. Sci.,* **50,** 1148–1151.

——, 1994: The Eady Problem for a basic state with zero PV gradient but $\beta \neq 0$. *J. Atmos. Sci.,* **51,** 3221–3226.

——, and A. Y. Hou, 1988: Hadley circulations for zonally averaged heating centered off the equator. *J. Atmos. Sci.,* **45,** 2416–2427.

——, and W. Pan, 1994: A note on orbital control of equator–pole heat fluxes. *Climate Dyn.,* **10,** 49–57.

Marshall, J. C., and A. J. G. Nurser, 1991: A continuously stratified thermocline model incorporating a mixed layer of variable thickness and density. *J. Phys. Oceanogr.,* **21,** 1780–1792.

Sun, D.-Z., and R. S. Lindzen, 1994: A PV view of the zonal mean distribution of temperature and wind in the extratropical troposphere. *J. Atmos. Sci.,* **51,** 757–772.